CIGI QUALITA MOSIM 2023
Geometric and dimensional inspection of maraging samples manufactured by Laser Powder Bed Fusion

AMANDA ROSSI DE OLIVEIRA[1], HENRIQUE LOPES DE CASTRO[2], SYDNEY FERREIRA SANTOS[3], ERIK GUSTAVO DEL CONTE[4]

[1]FEDERAL UNIVERSITY OF ABC, ENGINEERING, MODELING AND APPLIED SOCIAL SCIENCES CENTER
Avenida dos Estados, 5001, 09210-550, Santo André, São Paulo, Brazil
a.rossi@ufabc.edu.br

[2]FEDERAL UNIVERSITY OF ABC, ENGINEERING, MODELING AND APPLIED SOCIAL SCIENCES CENTER
Avenida dos Estados, 5001, 09210-550, Santo André, São Paulo, Brazil
henrique.castro@ufabc.edu.br

[3]FEDERAL UNIVERSITY OF ABC, ENGINEERING, MODELING AND APPLIED SOCIAL SCIENCES CENTER
Avenida dos Estados, 5001, 09210-550, Santo André, São Paulo, Brazil
sydney.ferreira@ufabc.edu.br

[4]FEDERAL UNIVERSITY OF ABC, ENGINEERING, MODELING AND APPLIED SOCIAL SCIENCES CENTER
Avenida dos Estados, 5001, 09210-550, Santo André, São Paulo, Brazil
erik.conte@ufabc.edu.br

***Résumé* – Les techniques de fabrication additive s'appliquent à toutes les classes de matériaux et ils offrent des opportunités d'innovation, élargissent les limites de la forme des pièces établies par la fabrication soustractive. La fusion laser sur lit de poudre (FLP) est l'une des techniques de fabrication additive capable produire des composants métalliques avec des géométries très complexes, qui seront de plus en plus demandée par l'industrie. Toutefois, la performance de la FLP est toujours sensible à certains paramètres de fabrication et peut ne pas satisfaire certaines exigences dimensionnelles et de finitions des surfaces. Ainsi, la présente étude visait à inspecter les attributs géométrique et dimensionnelle des spécimens d'acier maraging construits à trois emplacements de plaque de construction. Une machine de mesure de coordonnées (MMC) a été utilisé pour évaluer la planéité, un microscope confocal pour la rugosité et un micromètre pour la précision dimensionnelle. Il été vérifié une variation allant 8,6% de la précision de la largeur en fonction de l'emplacement de construction, tandis que la planéité et la rugosité n'ont pas changé de manière significative. Ces résultats contribueront à la gestion de la qualité des composants fabriquées par FLP, fournissant des informations pour la planification des futures voies de fabrication.**

***Abstract* – Additive Manufacturing technologies encompass the processing of all material classes and open up innovation opportunities, loosening part shape limits stated by subtractive processes. Laser Powder Bed Fusion (L-PBF) is one of the additive manufacturing techniques able to process metal components with high-complex geometries, which will be increasingly claimed in industry. Nevertheless, L-PBF performance is still sensitive to some processing parameters and may not satisfy some dimensional and finishing demands. So, the present study aimed to inspect the geometrical and dimensional attributes of maraging steel samples built in three platform locations. A coordinate measuring machine (CMM) was used for flatness evaluation, a laser confocal microscope for roughness, and a micrometer for dimensional accuracy analysis. 8.6% variation in width accuracy was verified depending on the build location, while flatness and surface roughness did not change significantly. These findings will contribute to the quality management of L-BPF manufactured components, providing insights for future process planning.**

***Mots clés* - précision dimensionnelle, fabrication additive, planéité, rugosité.**
***Keywords* – dimensional accuracy, additive manufacturing, flatness, roughness.**

1 INTRODUCTION

Data became an imperative factor in industry evolution, which needs to be adequately collected, exchanged between manufacturing components, and interpreted to support decision-making [Klingenberg et al., 2019]. A range of breakthrough technologies has been investigated to supply the demanding expertise, like the Internet of Things (IoT), Big Data, Cloud Computing, Artificial Intelligence, Cybersecurity, and Additive Manufacturing (AM) [Haleem et Javaid, 2019; Klingenberg et al., 2019]. Regarding AM technologies, a manufacturing paradigm shift is expected as soon as the AM reaches its plateau of productivity with a data-driven strategy to manage high-quality products manufacturing [Elambasseril et Brandt, 2022; Haleem et Javaid, 2019; Prashar et al., 2022].
The principle of AM techniques is layer upon layer building [ASTM International, 2021], encompassing standard steps for

operation. Firstly, it is needed the computer aided design (CAD) of the desired part for manufacturing [Gibson et al., 2015]. Secondly, the designed model should be converted into a Standard Triangle Language file, known as STL, which supplies information about the part surfaces and allows its computational slice for fabrication [Gibson et al., 2015]. Then, the file is transferred to the machine, and further programming of the manufacturing conditions, like the build platform location, can be determined using a computer aided manufacturing (CAM) environment [Gibson et al., 2015]. Then, the machine is physically and computationally set up to build the part. After manufacturing, the product may need a support removal, and a postprocessing stage, depending on the final application [Gibson et al., 2015].

AM technologies would provide extensive gains for different players in the production chain, benefiting the industry's evolution. This technology allows obtaining near-net-shape components by using just the necessary material. So, lead times and waste can be reduced based on the essence of the AM value stream mapping [Prashar et al., 2022]. Additionally, AM is one of the technologies that enable mass customization. Modular production and flexibility without significant changes in the production process are advantages of this manufacturing alternative. Nevertheless, the business case of additive manufacturing technologies needs to be addressed considering the technology potentials and limitations.

Laser Powder Bed Fusion (L-PBF) is one of the AM technologies in which the bulk component arises from the powder material through a laser beam responsible for fusing the powder and consolidating the building layers [ASTM International, 2021]. Although the benefits mentioned above, the AM of metals still needs further investigation regarding part quality, given that dimensional deviations and surface roughness limit the full potential of AM of metals [Haleem et Javaid, 2019].

There are few strategies able to manage the finishing issue yet. Laser surface remelting (LSR) is a known way to enhance the surface quality of L-PBF manufactured parts in an on-machine manner [Boschetto et al., 2021; Yasa et al., 2011]. In this operation, already-fused layers are remelted without adding material to reduce roughness or mitigate laser-induced defects [Boschetto et al., 2021], but strict tolerances can still not be met. Besides the LSR, other manufacturing parameters can influence the surface roughness of L-PBF, like the build orientation [Oliveira et Del Conte, 2021] and the laser focus shift [Bean et al., 2018]. So, it is crucial to investigate how processing parameters affect the quality of the final products to step on them.

Dimensional accuracy can also be affected by manufacturing conditions. Veetil et al. [2021] investigated how the platform location could influence the shrinkage and dimensional deviation of 316 L stainless steel samples. The authors reported a better circularity of cylindrical samples in locations farther from the gas inlet during a build cycle, explaining its findings with the gas effects on the solidification process [Veetil et al., 2021]. Thus, the quality management of L-PBF parts needs to consider process planning as a potential path for tuning final geometrical attributes.

Maraging steel is an age-hardenable martensitic alloy known by its high mechanical strength and ductility. This material can meet its expected mechanical performance when processed by L-PBF [Tan et al., 2017]. So, this steel was selected for the study, considering its importance in aerospace and aircraft structural components, such as helicopter shafts [Hall et Slunder, 1968], and also for tooling and molds [Bai et al., 2018], applications in which rigorous quality requirements in terms of geometric and dimensional accuracy need to be met.

In this context, the present study focused on inspecting the flatness, dimensional accuracy, and roughness of maraging steel samples built in three platform locations along the protection gas flow during L-BPF. It was possible to map the surface with 121 collection points using CMM and approximate a plane using the Least Square Error fitting to determine the flatness. The width and length dimensions of the cubic samples were also inspected with a digital micrometer for accuracy evaluation. Moreover, the area roughness S_a was analyzed on the remelted upper surfaces of the maraging samples. The proposed inspection analyses will contribute to verifying if the build platform location could influence these key attributes, thus supporting future L-PBF process planning depending on the product tolerances.

2 MATERIALS AND METHODS

Gas-atomized maraging powder supplied by Carpenter Additive (Cheshire, United Kingdom) was used as the raw material for the L-PBF process. Particle dimensions distribution had a diameter D50 of 29.2 μm [Carpenter Additive, 2021]. The main elements present in the material chemical composition are shown in Table 1.

Table 1. Main elements (>0.1 wt.%) on maraging powder.

Element	Ni	Co	Mo	Ti	Fe
wt.%	18.10	9.10	4.85	0.87	Balance

Source: Adapted from Carpenter Additive [2021].

EOSINT M280 machine was used for the L-PBF manufacturing of 10x10x10 mm cubic maraging samples in different platform locations (Figure 1). The laser scan strategy was the zig-zag rotated at 67º between layers. Some L-PBF processing parameters are shown in Table 2.

Table 2. L-PBF processing parameters.

Laser power	Beam diameter	Hatch distance	Stripe width	Layer thickness
170 W	0.1 mm	0.1 mm	5 mm	0.2 mm

The protection gas used for the building cycle was the N_2, which flew from the build chamber's back to front in the M280 machine, according to the inlets and outlet illustrated in Figure 1. Additionally, the last three layers of the cubic samples were subjected to LSR to improve the surface quality. Finally, electrical discharge machining took the samples out of the build platform.

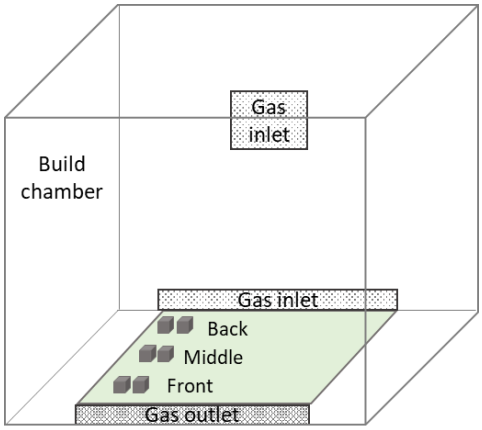

Figure 1. Illustrative scheme of the three studied platform positions.

2.1 Flatness evaluation plan

A Hexagon 4.5.4 Shop Floor CMM (Stockholm, Sweden) with a Ø1 mm ball tip touch probe was used for the upper surface mapping performed for flatness investigation, as shown in Figure 2a. The top surface from the CAD model was the reference to the CMM probe, defined in the PC-DMIS Hexagon software. Firstly, a calibration step was performed with nine points centered on the surface according to a 3x3 matrix with points spaced 1.5 mm apart. Then, the surface mapping was effectively executed with 121 points collected based on an 11x11 matrix with points spaced 1 mm apart, as illustrated in Figure 2. This procedure was performed for two samples in each platform location. The measurement uncertainty is 0.003 mm.

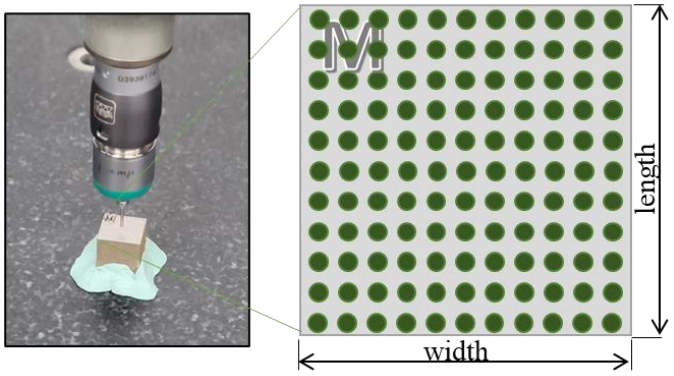

Figure 2. Experimental inspection of flatness with the surface mapping strategy used in CMM.

Considering the presence of the identification letters in the upper left corner of the evaluated surface (Figure 2), observed points of contact with such protuberances were disregarded for the flatness determination. So, the collected data were analyzed in MATLAB using the curve fitting toolbox. A least-square error fitting was run with a linear polynomial to obtain the mean plane of the flatness errors [Haitjema et Planes, 2016; Hexagon, 2020]. Then, the flatness was calculated based on the distance of the peak-to-valley points regarding the fitted equation coefficients. Finally, the influence of the build location on flatness was statistically evaluated with the Analysis of Variance (ANOVA) under a confidence level of 0.95.

2.2 Dimensional accuracy measurements

The dimensional accuracy of the cubic samples was determined by measuring the width and length of three points near the corners and middle of the sample height using a digital micrometer pantec IP54 (Ruggell, Liechtenstein) with a 0.001 mm resolution. Hence, dimensional accuracy was determined for each studied build location, considering the absolute difference between the average measurements and the nominal dimensions of 10 mm for both width and length [Cao et al., 2021]. The obtained results were used for the average and standard deviation calculations. As performed for flatness, the influence of the build location on dimensional accuracy was statistically evaluated with ANOVA.

2.3 Roughness measurements

The upper surface of the cubic samples, also used for flatness evaluation, was subjected to roughness investigation. Using a laser confocal microscope Olympus Lext OLS4100 (Tokyo, Japan), the area roughness arithmetic mean height (S_a) could be obtained from a 20x magnification stitching scan of the surface topographies using the LEXT software. Roughness values were obtained considering a cutoff of 0.8 mm, an evaluation length of 4 mm, and the correction of inclination and jagged errors. Again, the influence of the build location on roughness was statistically evaluated with ANOVA. Figure 3 shows the experimental setup for roughness determination.

Figure 3. Experimental inspection of roughness using the laser confocal.

3 Results and Discussions

3.1 Flatness evaluation

Figure 4 shows the points mapped in the upper surface of the samples in addition to fitted plans for each condition. Points above the fitting plane are mainly observed near the contour of the samples, especially for the front and middle located samples, giving rise to a more pronounced concave-like surface (Figure 4b,d,f). This shape is related to the thermal history experienced by the remelted surfaces during L-PBF. The temperature gradient mechanism, for instance, tends to induce residual stresses (and strains) depending on the heating and cooling responses of the material [Mercelis et Kruth, 2006]. This process is explained by the thermal expansion limitations imposed on the material by subjacent layers during heating, followed by a contraction during cooling [Mercelis et Kruth, 2006]. So, this phenomenon can be a major reason for the center contraction relative to the contours.

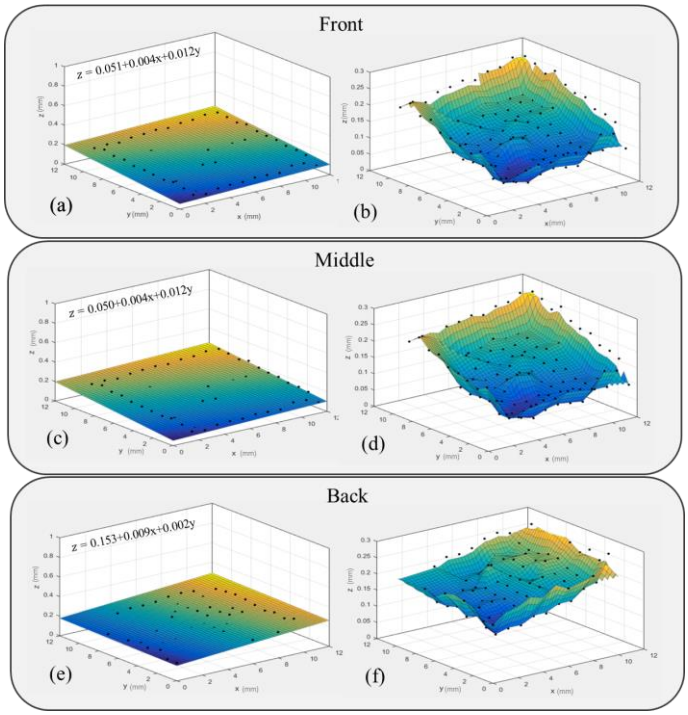

Figure 4. (a,c,e) Fitted planes for flatness evaluation and (b,d,f) surface linear interpolation based on mapped points.

Table 3 shows the flatness errors determined from the experimental points and fitted planes (Figure 4). Similar average flatness was found for the three build locations, showing relative independence on this processing parameter under the evaluated conditions. This observation was further validated with the p-value > 0.05 obtained with ANOVA (Table 4). Degrees of freedom (df) in ANOVA depend on the number of runs and evaluated levels for each factor. So, the residues df shown in Table 4 derive from the deduction of the build platform location degrees of freedom plus one from the six flatness measurements.

Table 3. Average calculated flatness.

Build platform location	Front	Middle	Back
Flatness (mm)	0.11 ± 0.03	0.09 ± 0.00	0.09 ± 0.01

Table 4. ANOVA for flatness.

Factor	Degrees of Freedom	Sum of Squares	F statistics	p-value
Build platform location	2	0.0007	1.14	0.43
Residues	3	0.0009	-	-

Considering the flatness errors (Table 3), it can be observed that the studied conditions of L-PBF could coarsely meet a tolerance of 0.1 mm, corresponding to 1% of the nominal cubic dimensions. This finding highlights slightly lower flatness errors than the ones found for horizontal walls of 718 Inconel samples in the literature [Gruber et al., 2020]. So, the processing parametrization used in the present study benefited the flatness.

3.2 Dimensional accuracy analysis

Table 5 depicts the average width and length accuracies for the maraging cubic samples regarding the nominal dimensions. The accuracy of the evaluated dimensions showed excellent stability within the replicates, considering the low standard deviations found for all cases. However, width presented slightly higher dimensional variations than length, based on the average values obtained for each build location.

Table 5. Average dimensional accuracy.

Build platform location	Front	Middle	Back
Width accuracy error (mm)	0.122 ± 0.004	0.112 ± 0.002	0.113 ± 0.006
Length accuracy error (mm)	0.096 ± 0.009	0.090 ± 0.005	0.102 ± 0.005

Tables 6 and 7 show the ANOVA performed for the width and length accuracies. Statistical results showed that the build platform location only affected the width dimensional accuracy due to the p-value lower than 0.5 (Table 6). In both cases, the degrees of freedom were six because of the nine measurements of length and width dimensional accuracy regarding the build location levels.

Table 6. ANOVA for width dimensional accuracy.

Factor	Degrees of Freedom	Sum of Squares	F statistics	p-value
Build platform location	2	0.00019	5.589	0.0426
Residues	6	0.00010	-	-

Table 7. ANOVA for length dimensional accuracy.

Factor	Degrees of Freedom	Sum of Squares	F statistics	p-value
Build platform location	2	0.00023	2.585	0.1550
Residues	6	0.00027	-	-

Thus, the more expressive variation related to the build location refers to the front location, in which the width dimensional accuracy errors were about 8.6% higher than the observed for the middle and back located samples, as shown in Figure 5. Considering the laser rotational scan strategy, the main factors expected to be related to these observations are the protection gas flow and its different capacities to remove by-products along the build chamber [Ladewig et al., 2016]. This hypothesis emerged from the fact that this was the indirect variable parameter when comparing the front located

samples with the others. However, further analysis of this phenomenon is required to conclude the remarkable consequences of this change.

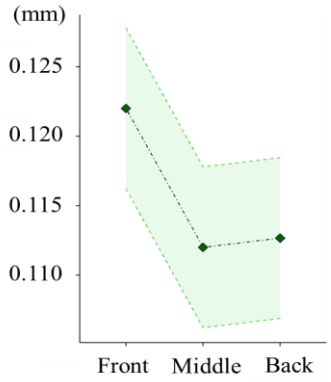

Figure 5. Main factor effects plot for width accuracy.

3.3 Roughness results

Figure 6 shows the remelted upper surface of the samples manufactured in the different build platform locations. Laser scan melt tracks are visible in all samples, but the back located one has better well-defined tracks. This observation may indicate the ease of removing by-products near the gas inlet (back), considering the possibility of redeposition of these elements on other regions along the gas flow [Ladewig et al., 2016].

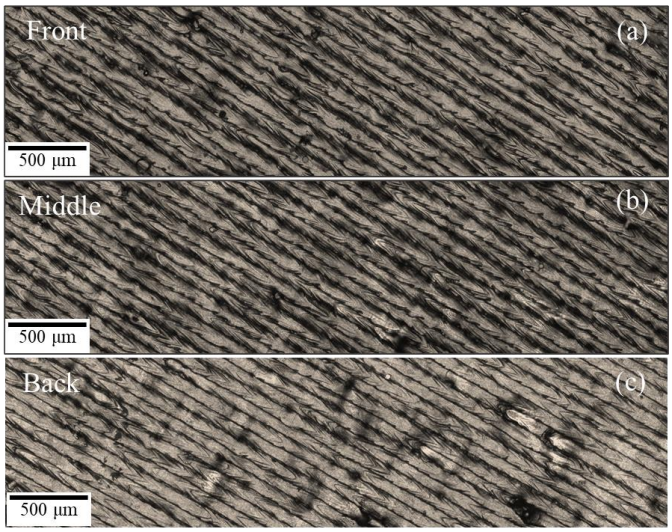

Figure 6. Remelted surfaces for the three build locations.

Table 8 details the average and standard deviation values found for the area roughness of the different located samples. Numerical results show that S_a did not vary with the build platform location when using the LSR. This consideration was reinforced by the p-value higher than 0.05 found with ANOVA (Table 9).

Table 8. Average roughness.

Build platform location	Front	Middle	Back
Upper surface S_a (µm)	4.3 ± 0.1	4.0 ± 0.5	4.1 ± 0.7

Roughness is expected to vary with L-PBF parameters when the surface is differently influenced. In this sense, can be cited, for instance: (a) by-products in the surroundings of the sample due to atmosphere instabilities from the interaction between laser and protection gas [Bean et al., 2018; Ladewig et al., 2016]; (b) the amount of unmolten powder particles stuck in the surface; or (c) the discretization of inclined/curved surfaces for manufacturing [Chen et al., 2018]. So, considering the found S_a, it can be pointed out that the LSR could homogenize this micro geometric feature of the surface for different build locations.

Table 9. ANOVA for roughness.

Factor	Degrees of Freedom	Sum of Squares	F statistics	p-value
Build platform location	2	0.1	0.27	0.77
Residues	6	1.3	-	-

3.4 Experimental data for artificial intelligence applications

Experimental data about additively manufactured samples can boost the capabilities of artificial intelligence technologies to control manufacturing systems [Elambasseril et Brandt, 2022]. This observation can be associated with the need to find out which processing parameters effectively affect properties of interest in the final products. Thus, the performed ANOVAs allowed the identification that only the width dimensional accuracy depended on the build platform location within a statistical confidence interval of 95% in the present study.

Even the development of robust artificial intelligence (AI) implementations can face the issue of obtaining representative data of the manufacturing systems [Elambasseril et Brandt, 2022; Klingenberg et al., 2019]. In this path, the proposed analysis can benefit feature dimensionality reductions on AI applications, depending on the response variable, considering that the evaluated properties showed different influences from the build platform location. This observation is of great interest due to the open issue of high dimensionality faced in additive manufacturing modeling [Liu, Tian et Kan, 2022]. So, the obtained experimental results should also be helpful to feed datasets under development for AI applications, as long as the surface roughness and geometric and dimensional features are important indicators of the L-PBF accuracy.

4 CONCLUSION

Flatness, dimensional accuracy, and roughness were inspected for maraging steel samples built in three platform locations along the protection gas flow during the L-BPF process. An average flatness of 0.1 mm was found, independent of the build location, relying on a tolerance of 1% of the nominal dimensions. Regarding the dimensional accuracy, while the length variation did not vary with the build location, the width accuracy was about 8.6% higher for the front located sample. Finally, the laser surface remelting favors an upper surface roughness of 4 µm for the front, middle, and back located samples. Depending on the build platform location, observed dimensional differences may relate to the protection gas effective removal of by-products. So, future studies will address a deep comprehension of the effects of protection gas flow regarding the build platform locations, especially in terms

of dimensional accuracy and other key properties. These findings will also generate L-PBF performance data for AI implementations.

5 ACKNOWLEDGMENTS

Project grants #2021/00553-6, #2021/09890-5, and #2022/00616-0, São Paulo Research Foundation (FAPESP).

6 REFERENCES

ASTM International. (2021). *ISO/ASTM 52900:2021 (en) Additive manufacturing — General principles — Fundamentals and vocabulary* (p. 38). Pennsylvania: ASTM.

Bai, Y., Yang, Y., Xiao, Z., & Wang, D. (2018). Selective laser melting of maraging steel: mechanical properties development and its application in mold. *Rapid Prototyping Journal*, *24*, 623–629. doi: 10.1108/RPJ-05-2017-0104

Bean, G. E., Witkin, D. B., McLouth, T. D., Patel, D. N., & Zaldivar, R. J. (2018). Effect of laser focus shift on surface quality and density of Inconel 718 parts produced via selective laser melting. *Additive Manufacturing*, *22*, 207–215. doi: 10.1016/j.addma.2018.04.024

Boschetto, A., Bottini, L., & Pilone, D. (2021). Effect of laser remelting on surface roughness and microstructure of AlSi10Mg selective laser melting manufactured parts. *The International Journal of Advanced Manufacturing Technology*, *113*, 2739–2759. doi: 10.1007/s00170-021-06775-3

Cao, L., Li, J., Hu, J., Liu, H., Wu, Y., & Zhou, Q. (2021). Optimization of surface roughness and dimensional accuracy in LPBF additive manufacturing. *Optics & Laser Technology*, *142*. doi: 10.1016/j.optlastec.2021.107246

Carpenter Additive. (2021). *Test Certificate - Gas Atomised M300 Maraging Steel LPBF (Flexible)* (p. 2). Portland Place.

Chen, Z., Wu, X., Tomus, D., & Davies, C. H. J. (2018). Surface roughness of Selective Laser Melted Ti-6Al-4V alloy components. *Additive Manufacturing*, *21*, 91–103. doi: 10.1016/j.addma.2018.02.009

Elambasseril, J., & Brandt, M. (2022). Artificial intelligence: way forward to empower metal additive manufacturing product development – an overview. *Materials Today: Proceedings*, *58*, 461–465. doi: 10.1016/j.matpr.2022.02.485

Gibson, I., Rosen, D., & Stucker, B. (2015). *Additive Manufacturing Technologies* (2nd ed.). New York, NY: Springer New York. doi: 10.1007/978-1-4939-2113-3

Gruber, S., Grunert, C., Riede, M., López, E., Marquardt, A., Brueckner, F., & Leyens, C. (2020). Comparison of dimensional accuracy and tolerances of powder bed based and nozzle based additive manufacturing processes. *Journal of Laser Applications*, *32*(032016). doi: 10.2351/7.0000115

Haitjema, H., & Planes, F. R. (2016). Flatness. In The International Academy for Production Engineering, L. Laperrière, & G. Reinhart (Eds.), CIRP Encyclopedia of Production Engineering. Berlin, Heidelberg: Springer Berlin Heidelberg. doi: 10.1007/978-3-642-35950-7

Haleem, A., & Javaid, M. (2019). Additive Manufacturing Applications in Industry 4.0: A Review. *Journal of Industrial Integration and Management*, *04*, 1930001-1–23. doi: 10.1142/S2424862219300011

Hall, A. M., & Slunder, C. J. (1968). The Metallurgy, Behavior, and Application of the 18-Percent Nickel Maraging Steels: A survey. *National Aeronautics and Space Administration*, *SP-5051*, 141.

Hexagon. (2020). *Flatness*. PC-DMIS Help Center - 2020.2. Retrieved from https://docs.hexagonmi.com/pcdmis/2020.2/en/helpcenter/index.htm#t=mergedProjects%2Fcore%2Fgeometric_tolerances%2FFlatness.htm

Klingenberg, C. O., Borges, M. A. V., & Antunes Jr, J. A. V. (2019). Industry 4.0 as a data-driven paradigm: a systematic literature review on technologies. *Journal of Manufacturing Technology Management*, *32*(3), 570–592. doi: 10.1108/JMTM-09-2018-0325

Ladewig, A., Schlick, G., Fisser, M., Schulze, V., & Glatzel, U. (2016). Influence of the shielding gas flow on the removal of process by-products in the selective laser melting process. *Additive Manufacturing*, *10*, 1–9. doi: 10.1016/j.addma.2016.01.004

Liu, C., Tian, W., & Kan, C. (2022). When AI meets additive manufacturing: Challenges and emerging opportunities for human-centered products development. *Journal of Manufacturing Systems, 64*, 648–656. doi: 10.1016/j.jmsy.2022.04.010

Mercelis, P., & Kruth, J. P. (2006). Residual stresses in selective laser sintering and selective laser melting. *Rapid Prototyping Journal*, *12*(5), 254–265. doi: 10.1108/13552540610707013

Oliveira, A. R. de, & Del Conte, E. G. (2021). Concurrent improvement of surface roughness and residual stress of as-built and aged additively manufactured maraging steel post-processed by milling. *The International Journal of Advanced Manufacturing Technology*. doi: 10.1007/s00170-021-07527-z

Prashar, G., Vasudev, H., & Bhuddhi, D. (2022). Additive manufacturing: expanding 3D printing horizon in industry 4.0. *International Journal on Interactive Design and Manufacturing (IJIDeM)*. doi: 10.1007/s12008-022-00956-4

Tan, C., Zhou, K., Ma, W., Zhang, P., Liu, M., & Kuang, T. (2017). Microstructural evolution, nanoprecipitation behavior and mechanical properties of selective laser melted high-performance grade 300 maraging steel. *Materials and Design*, *134*, 23–34. doi: 10.1016/j.matdes.2017.08.026

Veetil, J. K., Khorasani, M., Ghasemi, A., Rolfe, B., Vrooijink, I., Van Beurden, K., Moes, S., & Gibson, I. (2021). Build position-based dimensional deviations of laser powder-bed fusion of stainless steel 316L. *Precision Engineering*, *67*(2020), 58–68. doi: 10.1016/j.precisioneng.2020.09.024

Yasa, E., Deckers, J., & Kruth, J. (2011). The investigation of the influence of laser remelting on density, surface quality and microstructure of selective laser melting parts. *Rapid Prototyping Journal*, *17*(5), 312–327. doi: 10.1108/13552541111156450